frontiers in Materials

ORIGINAL RESEARCH
published: 09 April 2019
doi: 10.3389/fmats.2019.00054

Performance of Na-ion Supercapacitors Under Non-ambient Conditions—From Temperature to Magnetic Field Dependent Variation in Specific Capacitance

*Sudipta Biswas, Ananya Chowdhury and Amreesh Chandra**

Department of Physics, Indian Institute of Technology Kharagpur, Kharagpur, India

Single phase $NaFePO_4$ can works as economically viable cathode material for Na-systems similar to $LiFePO_4$–a material that led to the commercialization of Li-ion based energy systems. The reported microstructures of hollow $NaFePO_4$ particles, with porous walls, establish their advantages over solid morphologies. The hollow structures deliver stable electrochemical specific capacitance of 115 F g^{-1} in 2 M NaOH electrolyte, over a large number of cycles. This observation is directly attributed to the increased surface area, transport channels and redox sites, which become available in the porous-hollow particles. Hitherto unreported electrochemical performance under non-ambient environment is also discussed. In contrast to recently reported in Fe-based metal oxides, where significant change in specific capacitance has been reported as a function of magnetic field, it is observed that $NaFePO_4$ can protect itself and suppress modifications. More importantly, $NaFePO_4$ can work as an efficient electrode material in the temperature range RT to 65°C, which makes it useful for automotive industry.

Keywords: electrochemical, non-ambient conditions, hollow structure, energy storage, supercapacitor

OPEN ACCESS

Edited by:
Yuanlong Shao,
King Abdullah University of Science and Technology, Saudi Arabia

Reviewed by:
Liang Zhou,
Wuhan University of Technology, China
Wei Kong Pang,
University of Wollongong, Australia

****Correspondence:***
Amreesh Chandra
achandra@phy.iitkgp.ac.in

Specialty section:
This article was submitted to Energy Materials, a section of the journal Frontiers in Materials

Received: *15 January 2019*
Accepted: *18 March 2019*
Published: *09 April 2019*

Citation:
Biswas S, Chowdhury A and Chandra A (2019) Performance of Na-ion Supercapacitors Under Non-ambient Conditions—From Temperature to Magnetic Field Dependent Variation in Specific Capacitance. Front. Mater. 6:54. doi: 10.3389/fmats.2019.00054

INTRODUCTION

The rapidly expanding consumer market of mobile and wearable electronics is driving the research for supplementary energy storage systems, which can complement or even compete with Li-ion technologies. A recent statistical study has predicted that the energy storage capacity required only by mobile technologies like phone, tablets and laptops will be more than 25 GW h by 2025[1]. For the major part of the last 4 decades, Na-ion based energy storage systems remained under the shadow of their more illustrious counterparts based on Li-ion (Zhao et al., 2011). Infact, careful examination of literature shows that Na-ion energy storage systems (ESS) were actually investigated before Li-ion technologies. In 1960s, Kummer and Weber of Ford Motor Co extensively investigated β-Al_2O_3 Na^+ion conducting solid electrolyte based battery, which eventually led to the development of sodium/sulfur technologies[2]. Even after large-scale commercialization of Li-batteries, it was always known that sodium, with similar oxidation state and electronic configuration, can deliver characteristics similar Li^+ based energy storage devices. The re-emergence of interests in Na-ion energy storage devices is also linked to the constraints associated with most Li-ion based materials/technologies (Zhang et al., 2017). These range from

[1]http://energystorage.org/system/files/attachments/esa_vision_2025_final.pdf 06-09-2018
[2]https://patentimages.storage.googleapis.com/1a/51/27/63e4b6a1229db4/US3413150.pdf 06-09-2018

geo-economical/political, availability, increasing demand, environmental impacts, and countering the IP protection.

The primary reason, which restricted the use of Na-ion based technologies, was the limited number of materials that could handle the chemistry of bigger ion like Na^+. The growing understanding and expertise to develop novel nanoparticles ranging from solid, hierarchical to hollow, has allowed the resurgence of Na-ion based energy storage systems (Yabuuchi et al., 2014; Fang et al., 2015; de la Llave et al., 2016; Guo et al., 2016; Wang et al., 2019; Zhu et al., 2019). Different sodium based materials viz. $Na_4Ti_5O_{12}$, $NaTiO_2$, $Na_2Ti_3O_7$, $Na_3V_2(PO_4)_3$, $Na_4Fe(CN)_6$, $NaVO_2$, etc., are now being investigated (Didier et al., 2011; Yin et al., 2012; Li et al., 2015; Guo et al., 2016),(Jiang et al., 2016).

It is well known that the discovery and fabrication of $LiFePO_4$ led to rapid commercialization of the Li-ion batteries (Liang et al., 2015). Similar to it, $NaFePO_4$ has been suggested as a promising cathode material for Na-ion batteries (Liu et al., 2018). The major problem associated with this material is related to the difficulty of synthesizing it in single phase. Recently, there have been reports that have presented synthesis protocols, which have led to single phase $NaFePO_4$ with simple morphologies and broad particle size

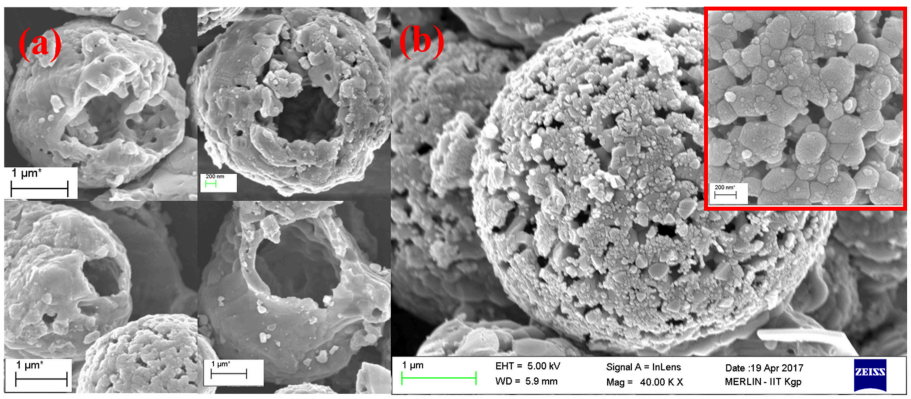

FIGURE 1 | (a) SEM image showing uniform microsphere, **(b)** SEM confirms porous and hollow structure.

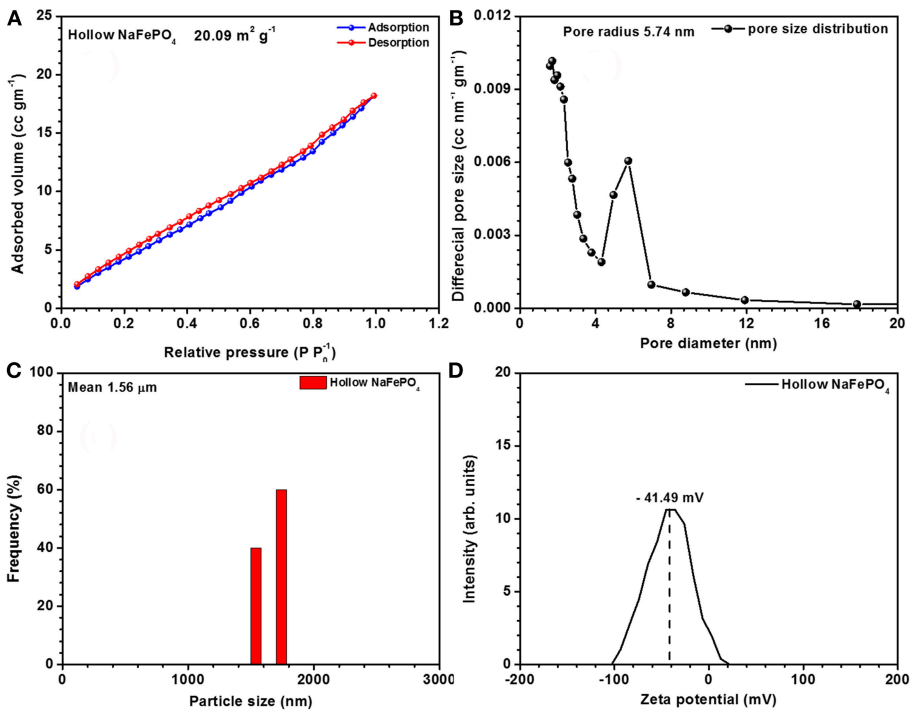

FIGURE 2 | (A) Adsorption-desorption isotherm curves, **(B)** pore size distribution curves, **(C)** particle size distribution, and **(D)** zeta potential curves of hollow $NaFePO_4$.

distributions (Minakshi et al., 2016; Rahman et al., 2017). The electrochemical response of these particles has been investigated only in batteries (Park et al., 2013; Slater et al., 2013). Typical energy densities that have been reported are ∼210–600 W h kg^{-1}. Intriguingly, its capacitive behavior remains ignored or mostly limited (Lu et al., 2015; Lim et al., 2016; Zhang et al., 2017; Ramakrishnan et al., 2018). For application in supercapacitors, tuning of morphology, surface area, pore size/dimension, and redox sites becomes essential.

In this paper, it is established that $NaFePO_4$ can also be used as efficient electrode material in supercapacitors, provided the morphology is carefully tuned. The results clearly prove that the hollow particles of $NaFePO_4$ have much higher capacitive behavior, in comparison to the solid counterparts. Superior performance of hollow structures can be attributed to the availability of more channels/sites for redox activities, while the enhanced surface area enforces increased contribution from the pseudo-capacitance (Sharma et al., 2018c).

Unlike the common strategy of reporting the supercapacitor response only at ambient conditions, the paper also discusses the behavior under non-ambient conditions. It is observed that $NaFePO_4$ can be easily used at elevated temperatures, which is essential if they are to be utilized in hybrid vehicles. The specific capacitance remains nearly same, even when the operating temperature is increased from RT to 65°C. Infact, slight increase in the specific capacitance is observed at elevated temperatures. The observation can be explained in terms of improved diffusion and accessibility of inner core for electrolyte ions insertion/de-insertion.

Very recently, few papers have indicated that Fe-based metal oxides used in supercapacitors will have to thoroughly re-characterized near magnetic field. Significant variation in specific capacitance can occur in such oxides as a function of varying dc-magnetic field, owing to modulated electron flow caused by the Lorentz force (Sharma et al., 2018a). It is demonstrated here that $NaFePO_4$ does show variation under magnetic field but the changes are much lower than that observed in pure Fe_2O_3. Therefore, $NaFePO_4$ based Na-ion capacitors can also be used near magnetic without disturbing the associated electronic circuitry.

EXPERIMENTAL

Material Used

Ferric nitrate nonahydrate ($Fe(NO_3)_3$, $9H_2O$), stearic acid, ammonium dihydrogen phosphate ($(NH_4)H_2PO_4$), tri-sodium citrate di-hydrate ($Na_3C_6H_5O_7$, $2H_2O$), citric acid, ethylene glycol, and sodium nitrate ($NaNO_3$) were procured from LobaChemie Pvt. Ltd. (India) and MerckSpecialities Pvt. Ltd. (India). All the analytical grade precursors were used directly without further purification.

Material Synthesis

Synthesis of Hollow and Porous structures

Porous and hollow $NaFePO_4$ microstructures were synthesized using one pot facile hydrothermal route followed by calcination in air. In a typical experimental procedure, 25 ml of 0.1 M ferric nitrate solution was mixed with 25 ml of 0.1 M stearic acid

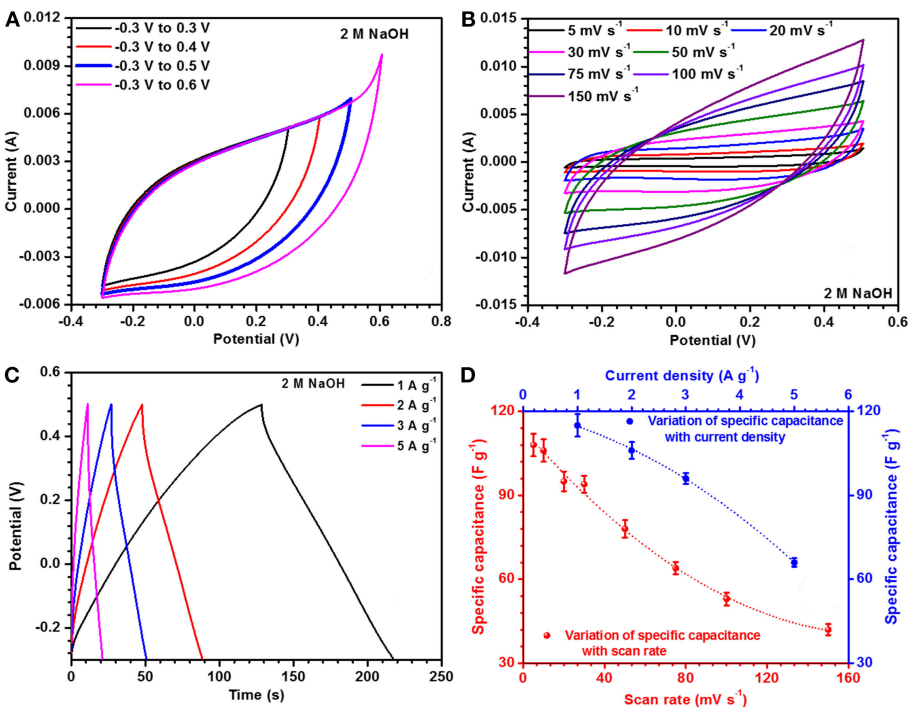

FIGURE 3 | (A) Window optimization, **(B)** CV profiles, **(C)** CD profiles, and **(D)** change in specific capacitance with scan rate and current density of hollow and porous $NaFePO_4$ in 2 M NaOH electrolyte.

solution. Subsequently, 245.1 mg trisodium citrate ($Na_3C_6H_5O_7$, $2H_2O$) was added and the solution was stirred for 2 h. Appropriate amount of ammonium dihydrogen phosphate ($(NH_4)H_2PO_4$) was added to the precursor solution so as to ensure Na:Fe:PO_4 concentration ratio was 1:1:1. 50 ml of this yellow colored solution was then transferred to a teflon-lined stainless steel (capacity 250 ml) autoclave. The autoclave was kept at 180°C for 24 h, before allowing it to slowly cool down to the room temperature. The precipitate was collected by centrifugation at 3,200 rpm. The precipitate was subsequentially washed three times using de-ionized water and dried overnight in a vacuum oven at 70°C. Dried sample was crushed and annealed at 600°C for 4 h in air to obtain hollow $NaFePO_4$ powder. To compare the performance of these hollow microstructures, solid nanoparticles of $NaFePO_4$ were also prepared. The corresponding synthesis protocol is given in the **Supplementary Information**.

Material Characterization

The phase formation of $NaFePO_4$ was confirmed by analyzing powder X-ray diffraction (XRD) profile obtained using a Rigaku MiniFlex600 diffractometer with Cu-Kα ($\lambda = 0.15406$ nm) as the incident wavelength.

For surface and particle morphological studies, both scanning and transmission electron micrographs were collected. For SEM data, CARL ZEISS SUPRA 40 SEM was used, while the TEM data were obtained utilizing a TEM FEI-TECHNAI G220S-Twin microscope operated at 200 kV. Brunauer-Emmett-Teller (BET) surface area and porosity were determined with a Quantachrome Nova Touch surface area and pore size analyzer. Zeta potential and particle size distribution were inferred by analyzing the DLS data obtained from a Horiba Scientific Nano Particle Analyzer SZ-100.

TABLE 1 | Specific capacitance of hollow and porous $NaFePO_4$ form CV curves in 2M NaOH electrolyte.

Scan Rate (mV s^{-1})	Specific Capacitance (F g^{-1})
5	108
10	106
20	95
30	94
50	78
75	64
100	53
150	42

TABLE 2 | Specific capacitance of hollow and porous $NaFePO_4$ form CD curves in 2M NaOH electrolyte.

Current Density (A g^{-1})	Specific capacitance (F g^{-1})
1	115
2	106
3	96
5	66

FTIR measurements were performed using Nexus 870 instrument in the range of 500–1,400 cm^{-1}. The spectrum was acquired in transmittance mode with a resolution of 1 cm^{-1}.

For the electrochemical characterization of the synthesized materials and fabricated devices, typical cyclic voltammetry (CV), and galvanostatic charge-discharge (GCD) were performed using the MetrohmAutolab (PGSTAT302N) potentiostat-galvanostat. The measurements were undertaken both in three- and two-electrode configurations, using an aqueous electrolyte. For impedance data of the electrochemical systems, in the frequency range of 50 mHz to 1 MHz, a N4L-PSM 1735 impedance analyzer was used.

Electrode Preparation and Electrochemical Characterization

A slurry was prepared by mixing 80 wt % active material, 10 wt % activated charcoal, and 10 wt % polyvinylidenefluoride-co-hexafluoropropylene (PVDF- HMP) using N-Methyl-2-pyrrolidone as the mixing media. All electrochemical measurements were performed in 1 M Na_2SO_4, 1 M $NaNO_3$, and 1 M NaOH electrolyte solutions, which allowed determination of an optimum electrolyte. Best performance was observed in NaOH and the corresponding results are presented in the paper. Platinum wire and Ag/AgCl/3.0 M KCl were used as the counter and reference electrodes, respectively.

RESULT AND DISCUSSION

It is now well established that, for useful electrochemically active materials, parameters such as: phase, particle morphology/size along with the nature of pores and pore-size/volume are critical (Singh and Chandra, 2015; Akhtar et al., 2016; Sharma et al., 2018b). The XRD plot obtained shown in **Figure S1** could be indexed using the *Pnmb* space group of $NaFePO_4$ following the JCPDS card no. 04-012-9665 (Kosova et al., 2014). XRD pattern for solid particle are shown in **Figure S2**.

Figures 1a,b shows the SEM micrographs of $NaFePO_4$ observed at various magnifications. It is clear that particles, with a cavity in the middle were stabilizing. Recently, hollow nanostructures of metal oxides have been suggested as electrode materials for next generation supercapacitors (Sharma et al., 2018b; Wei et al., 2018). Till date, there have been no reports, which have suggested formation of hollow $NaFePO_4$ particles/microspheres. The size of the synthesized $NaFePO_4$ microspheres varied in the range 1–3 μm. The micrographs also indicated that the wall surface of the hollow microspheres was not solid but porous. This can be an additional advantage of such particles because all the desired parameters i.e., surface area, pores, and transport channels, will be able to contribute in the final electrochemical reactions and/or specific capacitance. The particle growth mechanism is discussed in the supporting evidence (see **Figure S3**). The growth process was found to be a convoluted picture of reaction as well as diffusion kinetics. Corresponding SEM micrographs for solid $NaFePO_4$ structures are shown in **Figure S4** (see Supplementary Information).

The corresponding TEM images of the microspheres are given in supporting evidence (**Figure S5**). The associated elemental mapping and EDAX data for the $NaFePO_4$ microspheres are also described in the supporting evidence (**Figure S6**). The atomic ratio of Na:Fe:P:O was found to be 1.05:1:1.08:3.57, which confirmed the formation of $NaFePO_4$ with nominal composition and homogeneous distribution of the elements throughout the sample.

The surface area, pore size/volume and particle size distribution values are shown in **Figures 2A–D**. The BET adsorption-desorption curves showed typical type IV isotherms, indicating slit shaped mesopores of ∼6 nm. BET surface area was 20 m^2 g^{-1}.

Zeta potential denotes the electro kinetic potential in colloidal dispersions. In any chemical reaction, electro-positivity of the surface is determined by the overall pH of the solution. In the present studies, hollow nanostructures returned higher electro-positivity. This can only happen when there is an increased capacity to facilitate OH^- accommodation. This phenomenon helps to attract ions toward surface and hence increases the capacitance of the material. The surface charge (zeta potential) was −41.49 mV, as shown in **Figure 2D**.

It has been demonstrated that vibrational spectroscopy is very useful for probing fundamental sodium ion intercalation in a variety of crystalline sodium based electrode materials (Sharma et al., 2018c). The FTIR spectra of $NaFePO_4$ showed symmetric, asymmetric vibration as well as bending modes. The absorption bands at 1,009, 1,068, and 1,133 cm^{-1}, shown in the **Figure S7a**, could be assigned to the ν_3 type asymmetric stretching modes between P-O in PO_4^{3-}. The $\nu_1$modes near 980 and 947 cm^{-1} are attributed to the PO_4^{3-} intramolecular symmetric stretching vibrations (Sharma et al., 2018b). The asymmetric bending modes of the PO_4^{3-} anion, assigned as ν_4, were observed at 629, 577, and 540 cm^{-1} (see **Figure S7b**).

Before starting exhaustive electrochemical characterizations, it is critical to optimize the operating potential window. CV studies were performed at a scan rate of 50 mV s^{-1} in three different aqueous electrolytes viz., 1 M Na_2SO_4, $NaNO_3$, and NaOH. The mass of the electrode was kept at ∼1 mg. The observed CV curves in different voltage windows are shown in **Figures S8a–c**. The analysis clearly indicated that the electrolytes: Na_2SO_4 and $NaNO_3$ provided an electrochemical window ranging from −0.2 to 0.7 V. By using NaOH as electrolyte, voltage window of −0.3 to 0.5 V could be obtained. The CV curves as a function of varying scan rates, in the respective stabilized operational potential windows for the three electrolytes are shown in **Figures S8d–f**. After studying the electrochemical behavior of the hollow $NaFePO_4$ in three different electrolytes, NaOH was found to return the highest specific capacitance.

The estimated specific capacitance, with varying scan rates, is tabulated in **Table S1**. As expected, the specific capacitance showed appreciable dependence of the scan rates. The maximum specific capacitance, at 5 mV s^{-1} scan rate, was ∼75 F g^{-1} when 1 M NaOH electrolyte was used. When scan rate increased to 150 mV s^{-1} it was 20 F g^{-1}. The capacitance retention was found to be only ∼29%, when the scan rate was enhanced by 30 times.

The capacity to deliver the power of a commercial supercapacitor is obtained by the values of specific capacitance measured in galvanostatic charge discharge (CD) curves. The CD curves for the working electrode, in three different electrolytes are shown in **Figures S8g–i**.

The specific capacitance values, at different current densities, in three different electrolytes are listed in **Table S2**. The maximum capacitance of 87 F g^{-1} was obtained by using NaOH as electrolyte, which corroborated the results obtained from CV measurements. At higher specific currents, the specific capacitance decreased. This happens due to the underutilization of bulk capacitance, which is a normal behavior for supercapacitor electrode materials. At higher specific currents, the transfer of electrons toward the electrode is faster and hence the increase of potential would be higher. Consequently, the electrode gets reduced time to stay at a certain voltage and lower specific capacitance value is observed.

The electrolyte concentration has major effect on the electrochemical performance of an electrode material and is linked to the material's storage capacity. In the present case, the optimized concentration was found to be ∼ 2 M (NaOH). Operational window of the material was rechecked in 2 M NaOH and corresponding data is shown in **Figure 3A**. CV curves, at different scan rates, were collected in 2 M NaOH electrolyte and are shown in **Figure 3B**. Maximum specific capacitance was found to be 108 F g^{-1} at a scan rate of 5 mV s^{-1}. In the same potential window, CD profiles were also collected at different current densities. These are depicted in **Figure 3C**. The maximum specific capacitance in this case was found to be ∼115 F g^{-1} at 1 A g^{-1}. The specific capacitance values for the porous and hollow $NaFePO_4$, utilizing 2 M NaOH as electrolyte, at different scan rates and current densities are listed in **Tables 1**, **2**, respectively and corresponding graphs are shown in **Figure 3D**. It was also observed that the hollow structure based electrodes showed higher capacitance retention ability.

The performance of hollow structures was compared with that of $NaFePO_4$ solid particles. From the CV analysis, the maximum specific capacitance of 48 F g^{-1} was observed in the case of solid particles. The CD profiles gave the specific capacitance to be 81 F g^{-1}. Clearly, the hollow structures had much higher performance. The advantages of both outer/inner surfaces, low diffusion length, high availability of surface adsorption sites due to the hollow cavity of the particles would drive this enhanced performance. The CV and CD curves for solid structures are shown in **Figure S9** and the corresponding specific capacitance values are given in **Tables S3**, **S4**, respectively.

Cyclic stability of an electrode is one of the important property that decides its industrial application. In the present case, 93.7% of capacity retention was found after 1,500 cycles for hollow microsphere [see **Figure 4A**]. Solid structures also showed similar capacity retention after 1,500 cycles. This can be expected because the redox reactions would be similar as the chemical formula or composition was not varying as a function of particle morphology. The advantages rendered by hollow particles was leading to higher specific capacitance. Hollow and solid structures had BET surface areas of 20 and 6 m^2 g^{-1}, respectively. Hollow structures, with pore radius

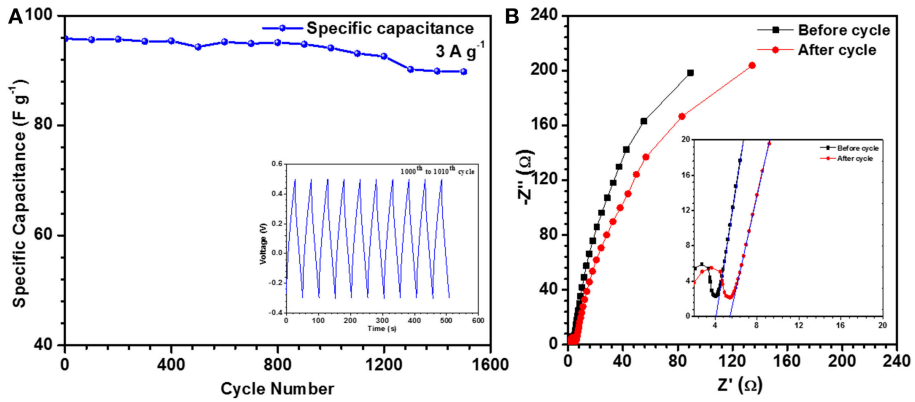

FIGURE 4 | (A) Cycling test for $NaFePO_4$ electrode and CD from 1,001 to 1,010 cycle (inset) and **(B)** EIS of hollow $NaFePO_4$.

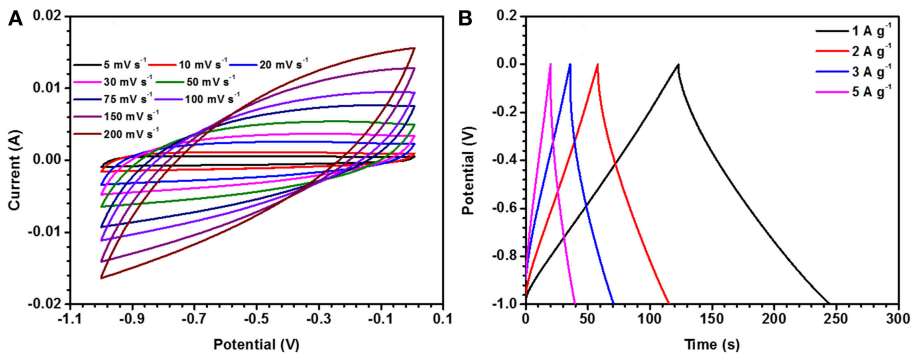

FIGURE 5 | (A) CV and **(B)** CD profiles for three electrode measurements of activated carbon (AC).

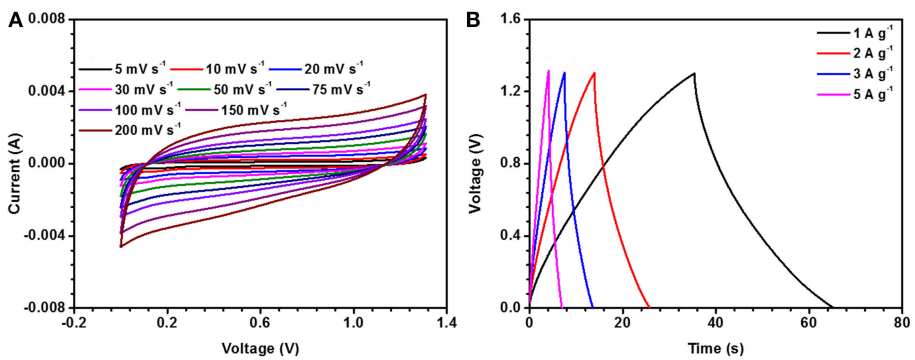

FIGURE 6 | (A) CV and **(B)** CD profiles of $NaFePO_4$//AC device at room temperature (25°C).

∼5.7 nm, would also allow better intercalation/ de-intercalation of electrolyte ions than the solid particles that showed pores of ∼1.7 nm radius. The surface area, pore size/volume, particle size distribution, and zeta potential of solid particles are depicted in **Figures S10a–d**.

The charge transport kinetics of the electrode was studied by the analysis of electrochemical impedance spectroscopy (EIS) data. Nyquist plots give the information about electrode-electrolyte interactions and equivalent series resistance (ESR). The ESR values for hollow microsphere and solid nanostructures were ∼4.0 Ω (**Figure 4B**) and ∼6.6 Ω (**Figure S11**), respectively. This indicated low charge transfer resistance at the working electrode and electrolyte interface in the case of hollow structures. Capacity retention for

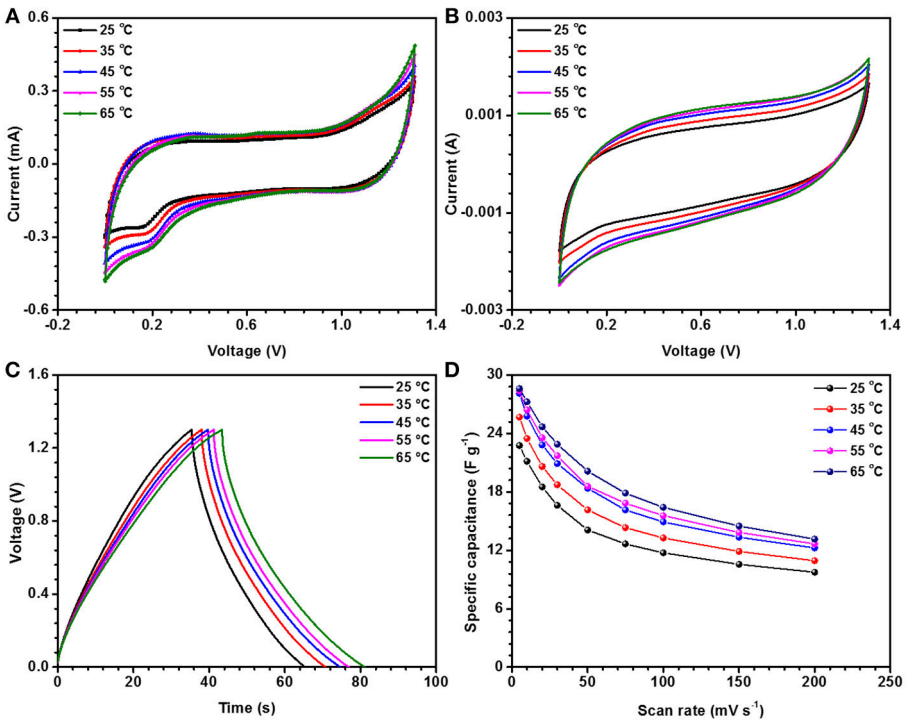

FIGURE 7 | CV measurements at different temperature for the device **(A)** at 5 mV s^{-1} and **(B)** at 50 mV s^{-1}, **(C)** CD measurements for $NaFePO_4$//AC device at different temperature, and **(D)** variation of specific capacitance with scan rate.

TABLE 3 | Values of specific capacitance at different scan rates at different temperature (screw cell device).

Scan rate (mV s^{-1})	Specific capacitance (F g^{-1})				
	Room temperature (25°C)	35°C	45°C	55°C	65°C
5	23	26	28	28	29
10	22	23	26	26	27
20	18	21	23	24	25
30	16	19	21	22	23
50	14	16	18	19	20
75	13	14	16	17	18
100	12	13	15	16	16
150	11	11	13	14	15
200	10	11	12	13	13

TABLE 4 | Values of specific capacitance at different current densities at different temperature (screw cell device).

Current Density (A g^{-1})	Specific capacitance (F g^{-1})				
	25°C (RT)	35°C	45°C	55°C	65°C
1	23	26	28	29	29
2	20	22	23	24	26
3	15	17	18	20	22
5	12	14	13	16	16

TABLE 5 | Values of resistance at different temperature.

Temperature (° C)	Resistance (Ω)
Room temperature (25)	7.63
35	7.49
45	7.30
55	6.94
65	6.52

hollow structures can be justified by the ESR measurements. The values of ESR increased from ∼4.0 to 5.4 Ω, in case of hollow $NaFePO_4$. This increment in the ESR values can be attributed to the electrode degradation and reduction in the available ion channels within the materials as a function of cycling. It is clear from the lower frequency regions in **Figure 4B**, that the capacitive behavior was lower in case of hollow structures.

Supercapacitor coin cell type device was fabricated using activated carbon as the negative and $NaFePO_4$ as the positive electrode. Activated carbon was tested in three-electrode configuration before making the device. **Figures 5A,B** shows the cyclic voltametric curves at different scan rates from 5 to 200 mV s^{-1} and charge discharge at different current density from 0.5 to 5 A g^{-1}. From the CV results, the working electrochemical window was found to be −1 to 0 V.

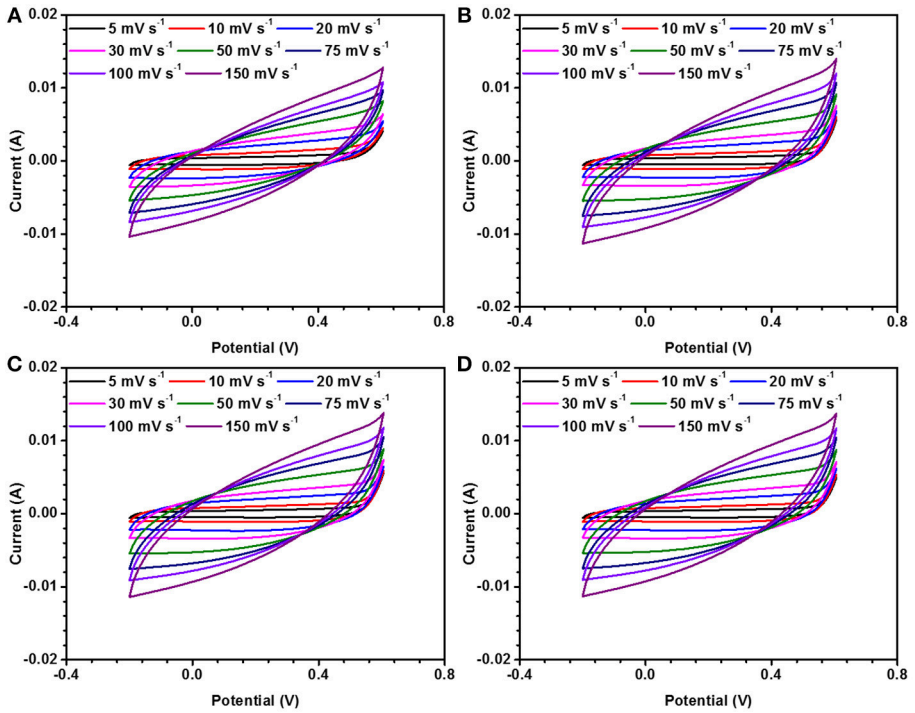

FIGURE 8 | CD measurements in three electrode set up for $NaFePO_4$ at **(A)** 0, **(B)** 10, **(C)** 20, and **(D)** 30 gauss magnetic field.

TABLE 6 | Values of specific capacitance at different scan rate under varying magnetic field (in three electrode configuration).

Scan rate (mV s^{-1})	Specific capacitance (F g^{-1})			
	No field	10 gauss	20 gauss	30 gauss
5	109	120	123	124
10	108	120	122	123
20	99	119	120	121
30	86	109	113	113
50	65	87	91	91
75	51	68	71	78
100	43	56	58	58
150	34	43	44	44

Highest specific capacitance observed from the CV measurement was 120 F g^{-1}, at a scan rate 5 mV s^{-1}. Using charge-discharge measurements, it was estimated as 126 F g^{-1} at current density of 1 A g^{-1}. Specific capacitance values from CV and CD for activated carbon are shown in **Tables S5**, **S6**, respectively.

Fabrication of asymmetric supercapacitor device needs charge balancing of the electrode materials. The optimal charge balance condition was estimated using the mass balance formula:

$$\frac{m_+}{m_-} = \frac{V_- C_-}{V_+ C_+} \quad (1)$$

where C_- and C_+ are the capacitances (in F g^{-1}) measured at the same scan rate, using the three electrode system, for negative and positive electrodes, respectively while ΔV_+ and ΔV_- denote the working potential window for the positive and negative electrodes, respectively. The required mass ratio for positive and negative electrode materials (m_+/m_-) was thus estimated as 1.5 at 5 mV s^{-1}.

Figure 6 shows the cyclic voltammetry and charge discharge curves for device. Whatman glass fiber paper was used as separator (pre-soaked in electrolyte) and 2 M NaOH was used as aqueous electrolyte. The electrochemical voltage window was found to be from 0 to 1.3 V. No H_2/O_2 evolution was discernible in this voltage window. From the CV measurements, maximum specific capacitance for the $NaFePO_4$//AC device was ~22 F g^{-1}. The device performance was found to decrease at higher scan rate, as a result of under-utilization bulk of the material. The maximum specific capacitance observed from CD was 23 F g^{-1}. Nearly linear charge discharge curves showed the dominance of the electric double layer capacitance (EDLC) in the device.

In most of the applications, there are few additional parameters, which contribute in determining the final electrochemical performance. These include: temperature, external frequency, magnetic field, etc., (Ramakrishnan et al., 2018; Sharma et al., 2018a). Till date, such studies have remained ignored in the Na-ion based supercapacitors. Given below are the performance of the $NaFePO_4$ based supercapacitors under variable temperature and magnetic field.

It has been suggested that, at elevated temperatures, contributions from additional factors such as ion conductivity, solubility limits, viscosity, thermal stability, etc., cannot be ignored. For investigating the thermal stability, the device was slowly heated at increments of 10°C. The device was equilibrated for 30 min at a given temperature before the electrochemical measurements were performed. As presented above, the specific capacitance in $NaFePO_4$ based screw cell type asymmetric device was ∼23 F g^{-1}. The CV and CD curves, with increasing temperature, are shown in **Figures S12**, **S13**. CV curves with increasing temperature at a scan rate of 5 and 50 mV s^{-1} are shown in **Figures 7A,B**, respectively. Comparison of charge discharge curve at 1 A g^{-1} with increase in temperature and variation of specific capacitance with scan rate is shown in **Figures 7C,D**, respectively. Clear signature was obtained, which suggested increase in the specific capacitance with increasing temperature. At 65°C, the specific capacitance increased to 29 F g^{-1}, which was nearly 25% higher than the value obtained at room temperature. Additionally, the device continued to show the characteristics expected from a capacitive system. The corresponding values of specific capacitance from CV and CD analysis are listed in **Tables 3**, **4**, respectively. The intrinsic internal resistance decreased with increasing temperature and the values are given in **Table 5**.

On comparing with literature dealing with elevated temperature behavior in supercapacitors fabricated using metal oxides, it was interesting to note that the Na-ion based device showed much lower variation as a function of temperature. This can be directly correlated with the fact that the olivine structures show much lower thermal expansion than the other relevant metal oxides. Therefore, change of ∼50°C will not lead to appreciable change in the surface area or pore structure in the $NaFePO_4$ particles. It is known that, with increasing temperature, the reaction kinetics increases. Therefore, in the Na-based olivines, the increase in specific capacitance with increasing temperature will only be dominated by the enhanced electrochemical reactions near the electrolyte-electrode interface, which will vary too much in the temperature window of ∼40°C.

It has been very recently reported that electrode materials based on ferromagentic ions may have to revisited because devices fabricated using them can have appreciable effect under/near variable magnetic field. $NaFePO_4$ also has Fe, which is a well-known ferromagnetic atom. The magnetic field dependent studies in $NaFePO_4$, while it is being used as an electrode material in storage device, has never been reported. Cyclic voltammetry (CV) and galvanostatic charge-discharge (CD) measurements were performed under varying magnetic fields (B = 0, 10, 20, and 30 gauss). CV curves at different scan rate and at different current densities under varying magnetic fields (B = 0, 10, 20, and 30 gauss) are shown in **Figure 8** and **Figure S14**. Schematic of experimental arrangement for performing the magnetic field dependent measurements is shown in **Figure S15** of the supplementary information. The calculated specific capacitance values are listed in **Table 5**. It was clear that the specific capacitance showed an increasing trend, with increasing magnetic field. On reaching the magnetic field of 30 gauss, the specific capacitance at 5 mV s^{-1} increased to 124 F g^{-1} from 109 F g^{-1}, which was observed at 0 Gauss. This corresponded to a mere 14% change. Additionally, no change was observed even by further increasing the magnetic field. In comparison, nearly 75% increase has been reported in Fe_2O_3 or MnO_2. So, $NaFePO_4$ clearly showed stability near magnetic field, which would make this material even more important for industrial use. The values of specific capacitance at different scan rates is shown in **Table 6** and corresponding specific capacitance values from charge discharge is shown in **Table S7**.

One of the reasons behind the increase in capacitance response in magnetic field is magneto hydrodynamic (MHD) effect. This increases the magnetic current in the system because of the feedback mechanism and increase in vigorous hydrodynamic stirring. Further, the change of electronic energy state due to the applied magnetic field may also improve the performance of electrode material. The suppressed magnetic field dependence can be easily explained if we examine the expected valence state of the elements in $NaFePO_4$. Fe is expected to be in a +2 state, which is known to be non-magnetic. If magnetism has to be induced in it then large magnetic field has to be applied as per the Van Vleck paramagnets (Smolenski et al., 2016). Additional, Na (valency +1) is a known diamagnetic. Therefore, it will oppose the realignment in transport channels, which may

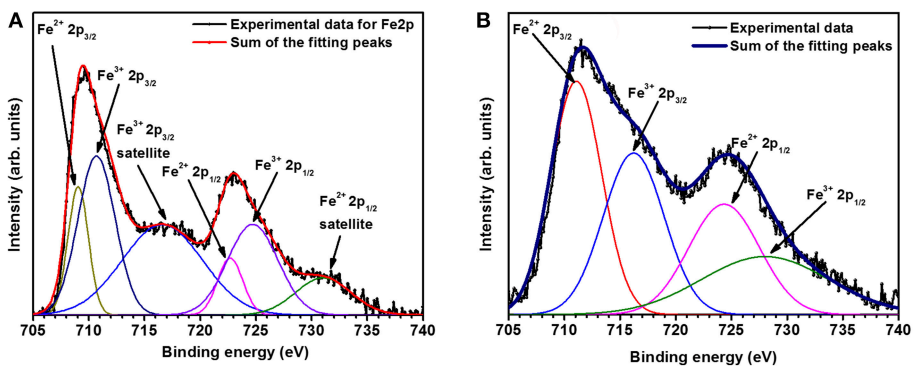

FIGURE 9 | XPS spectra for Fe present in (A) Fe_2O_3 and (B) $NaFePO_4$.

occur owing to structural reorientation driven by the magnetic iron (Fe^{3+}, which can also stabilize during material synthesis). To confirm the presence of ionized state of Fe analysis, XPS data was collected (shown in **Figure 9**) and analyzed. XPS result showed that the percentage of Fe^{2+} and Fe^{3+} was ∼55 and 45%, respectively, in $NaFePO_4$. As Fe^{2+} is nonmagnetic, Fe^{3+} drives the response under external magnetic field. The effect is more pronounced in Fe_2O_3 that had much higher percentage of Fe^{3+} (70%) with respect to the Fe^{2+} state (30%). This makes $NaFePO_4$ useful for application near the magnetic environment.

CONCLUSION

Single phase $NaFePO_4$ particles, with hollow cavity having porous walls, are reported. This microstructure allows efficient utilization of active surface area and pore structure, leading to high specific capacitance. Bulk structures return specific capacitance of ∼48 F g^{-1} at a scan rate 5 mV s^{-1} and 81 F g^{-1} at a current density of 1 A g^{-1}. For hollow microstructures structure, the specific capacitance is found to be 108 F g^{-1} at a scan rate 5 mV s^{-1} and 115 F g^{-1} at a current density 1 A g^{-1}. $NaFePO_4$ also shows long term stability under non-ambient conditions, where parameters such as magnetic field or temperature are varied. $NaFePO_4$ has the capacity to deliver performance similar to $LiFePO_4$ and make Na-ion based energy systems industrially and economically viable.

AUTHOR CONTRIBUTIONS

SB and AnC have contributed equally in sample preparation and data analysis under direct supervision of AmC as part of their Ph.D. program. AmC has also contribute in data analysis and interpretation.

FUNDING

MES program of the Department of Science and Technology, India.

ACKNOWLEDGMENTS

The authors acknowledge the financial support received from DST (India) under the MES scheme to pursue work under the project entitled: Hierarchically nanostructures energy materials for next generation Na-ion based energy storage technologies and their use in renewable energy systems.

SUPPLEMENTARY MATERIAL

The Supplementary Material for this article can be found online at: https://www.frontiersin.org/articles/10.3389/fmats.2019.00054/full#supplementary-material

REFERENCES

Akhtar, M. A., Sharma, V., Biswas, S., and Chandra, A. (2016). Tuning porous nanostructures of $MnCo_2O_4$ for application in supercapacitors and catalysis. *RSC Adv.* 6, 96296–96305. doi: 10.1039/C6RA20004D

de la Llave, E., Borgel, V., Park, K. J., Hwang, J. Y., Sun, Y. K., Hartmann, P., et al. (2016). Comparison between Na-ion and Li-ion cells: understanding the critical role of the cathodes stability and the anodes pretreatment on the cells behavior. *ACS Appl. Mater. Interfaces* 8, 1867–1875. doi: 10.1021/acsami.5b09835

Didier, C., Guignard, M., Denage, C., Szajwaj, O., Ito, S., Saadoune, I., et al. (2011). Electrochemical Na-deintercalation from $NaVO_2$. electrochem. *Solid-State Lett.* 14:A75. doi: 10.1149/1.3555102

Fang, Y., Liu, Q., Xiao, L., Ai, X., Yang, H., and Cao, Y. (2015). High-performance olivine $NaFePO_4$ microsphere cathode synthesized by aqueous electrochemical displacement method for sodium ion batteries. *ACS Appl. Mater. Interfaces* 7, 17977–17984. doi: 10.1021/acsami.5b04691

Guo, S., Yi, J., Sun, Y., and Zhou, H. (2016). Recent advances in titanium-based electrode materials for stationary sodium-ion batteries. *Energy Environ. Sci.* 9, 2978–3006. doi: 10.1039/C6EE01807F

Jiang, X., Yang, L., Ding, B., Qu, B., Ji, G., and Lee, J. Y. (2016). Extending the cycle life of $Na_3V_2(PO_4)_3$ cathodes in sodium-ion batteries through interdigitated carbon scaffolding. *J. Mater. Chem. A* 4, 14669–14674. doi: 10.1039/C6TA05030A

Kosova, N. V., Podugolnikov, V. R., Devyatkina, E. T., and Slobodyuk, A. B. (2014). Structure and electrochemistry of $NaFePO_4$ and Na_2FePO_4F cathode materials prepared via mechanochemical route. *Mater. Res. Bull.* 60, 849–857. doi: 10.1016/j.materresbull.2014.09.081

Li, W.-J., Chou, S.-L., Wang, J.-Z., Kang, Y.-M., Wang, J.-L., Liu, Y., et al. (2015). Facile method to synthesize Na-enriched $Na_{1+x}FeFe(CN)_6$ frameworks as cathode with superior electrochemical performance for sodium-ion batteries. *Chem. Mater.* 27, 1997–2003. doi: 10.1021/cm504091z

Liang, Y., Wen, K., Mao, Y., Liu, Z., Zhu, G., Yang, F., et al. (2015). Shape and size control of $LiFePO_4$ for high-performance lithium-ion batteries. *ChemElectroChem* 2, 1227–1237. doi: 10.1002/celc.201500114

Lim, E., Jo, C., Kim, M. S., Kim, M.-H., Chun, J., Kim, H., et al. (2016). High-performance sodium-ion hybrid supercapacitor based on Nb_2O_5@Carbon core-shell nanoparticles and reduced graphene oxide nanocomposites. *Adv. Funct. Mater.* 26, 3711–3719. doi: 10.1002/adfm.201505548

Liu, Y., Zhang, N., Wang, F., Liu, X., Jiao, L., and Fan, L.-Z. (2018). Approaching the downsizing limit of maricite $NaFePO_4$ toward high-performance cathode for sodium-ion batteries. *Adv. Funct. Mater.* 28:1801917. doi: 10.1002/adfm.201801917

Lu, K., Li, D., Gao, X., Dai, H., Wang, N., and Ma, H. (2015). An advanced aqueous sodium-ion supercapacitor with a manganous hexacyanoferrate cathode and a Fe_3O_4/rGO anode. *J. Mater. Chem. A* 3, 16013–16019. doi: 10.1039/C5TA04244E

Minakshi, M., Mitchell, D., Jones, R., Alenazey, F., Watcharatharapong, T., Chakraborty, S., et al. (2016). Synthesis, structural and electrochemical properties of sodium nickel phosphate for energy storage devices. *Nanoscale* 8, 11291–11305. doi: 10.1039/C6NR01179A

Park, Y. U., Seo, D. H., Kwon, H. S., Kim, B., Kim, J., Kim, H., et al. (2013). A new high-energy cathode for a Na-ion battery with ultrahigh stability. *J. Am. Chem. Soc.* 135, 13870–13878. doi: 10.1021/ja406016j

Rahman, M. M., Sultana, I., Mateti, S., Liu, J., Sharma, N., and Chen, Y. (2017). Maricite $NaFePO_4$/C/graphene: a novel hybrid cathode for sodium-ion batteries. *J. Mater. Chem. A* 5, 16616–16621. doi: 10.1039/C7TA04946C

Ramakrishnan, K., Nithya, C., and Karvembu, R. (2018). High-performance sodium ion capacitor based on MoO_2@rGO nanocomposite and goat hair derived carbon electrodes. *ACS Appl. Energy Mater.* 1, 841–850. doi: 10.1021/acsaem.7b00284

Sharma, V., Biswas, S., and Chandra, A. (2018a). Need for revisiting the use of magnetic oxides as electrode materials in supercapacitors: unequivocal evidence of significant variation in specific capacitance under variable magnetic field. *Adv. Energy Mater.* 2018:1800573. doi: 10.1002/aenm.201800573

Sharma, V., Singh, I., and Chandra, A. (2018b). Hollow nanostructures of metal oxides as next generation electrode materials for supercapacitors. *Sci. Rep.* 8:1307. doi: 10.1038/s41598-018-19815-y

Sharma, V., Singh, I., and Chandra, A. (2018c). Origin of superior catalytic activity in copper (II) oxide nanoflakes in comparison to solid or even hollow particles. Mater. *Lett*. 211, 285–288. doi: 10.1016/j.matlet.2017.10.030

Singh, A., and Chandra, A. (2015). Significant performance enhancement in asymmetric supercapacitors based on metal oxides, carbon nanotubes and neutral aqueous electrolyte. *Sci. Rep.* 5:15551. doi: 10.1038/srep15551

Slater, M. D., Kim, D., Lee, E., and Johnson, C. S. (2013). Sodium-ion batteries. *Adv. Funct. Mater*. 23, 947–958. doi: 10.1002/adfm.201200691

Smolenski, T., Kazimierczuk, T., Kobak, J., Goryca, M., Golnik, A., Kossacki, P., et al. (2016). Magnetic ground state of an individual Fe(2+) ion in strained semiconductor nanostructure. *Nat. Commun*. 7:10484. doi: 10.1038/ncomms10484

Wang, X., Niu, C., Meng, J., Hu, P., Xu, X., Wei, X., et al. (2019). Novel $K_3V_2(PO_4)_3$/C bundled nanowires as superior sodium-ion battery electrode with ultrahigh cycling stability. *Adv. Energy Mater*. 5, 1500716–1500723. doi: 10.1002/aenm.201500716

Wei, J., Li, X., Xue, H., Shao, J., Zhu, R., and Pang, H. (2018). Hollow structural transition metal oxide for advanced supercapacitors. *Adv. Mater. Interf*. 5:1701509. doi: 10.1002/admi.201701509

Yabuuchi, N., Kubota, K., Dahbi, M., and Komaba, S. (2014). Research development on sodium-ion batteries. *Chem. Rev*. 114, 11636–11682. doi: 10.1021/cr500192f

Yin, J., Qi, L., and Wang, H. (2012). Sodium titanate nanotubes as negative electrode materials for sodium-ion capacitors. *ACS Appl. Mater. Interfaces* 4, 2762–2768. doi: 10.1021/am300385r

Zhang, S., Liu, Y., Han, Q., He, S., Zhang, N., and Yang, J. (2017). Development and characterization of aqueous sodium-ion hybrid supercapacitor based on $NaTi_2(PO_4)_3$ //activated carbon. *J. Alloys Compd*. 729, 850–857. doi: 10.1016/j.jallcom.2017.08.256

Zhao, D. D., Wang, Y., and Zhang, Y. F. (2011). High-performance Li-ion batteries and supercapacitors based on prospective 1-D nanomaterials. *Nano-Micro Lett*. 3, 62–71. doi: 10.1007/BF03353653

Zhu, T., Hu, P., Wang, X., Liu, Z., Luo, W., Owusu, K. A., et al. (2019). Realizing three-electron redox reactions in NASICON-structured $Na_3MnTi(PO_4)_3$ for sodium-ion batteries. *Adv. Energy Mater*. 2019:1803436. doi: 10.1002/aenm.201803436

Conflict of Interest Statement: The authors declare that the research was conducted in the absence of any commercial or financial relationships that could be construed as a potential conflict of interest.